

Discrete deposition of hydroxyapatite nanoparticles on a titanium implant with predisposing substrate microtopography accelerated osseointegration

Ichiro Nishimura^{1,3}, Yuhong Huang², Frank Butz¹,
Takahiro Ogawa¹, Audrey Lin¹ and Chiachien Jake Wang¹

¹ UCLA School of Dentistry, The Weintraub Center for Reconstructive Biotechnology and Division of Advanced Prosthodontics, Biomaterials and Hospital Dentistry, Los Angeles, CA, USA

² Chemat Technology, Incorporated, Northridge, CA, USA

E-mail: ichiron@dent.ucla.edu

Received 21 March 2007, in final form 28 April 2007

Published 18 May 2007

Online at stacks.iop.org/Nano/18/245101

Abstract

We report here a new versatile method to deposit discrete hydroxyapatite (HA) nanoparticles on a titanium (Ti) implant with predisposing substrate microtopography, which exhibited an unexpectedly robust biological effect. Commercially pure Ti substrates were treated with 3-aminopropyltriethoxysilane, on which HA nanoparticles (20 nm) were deposited and chemically bonded to TiO₂. The HA deposition rate was linearly related to the treatment time and HA nanoparticles were deposited on up to 50% of the substrate surface. As a result, the discrete deposition of HA nanoparticles generated novel 20–40 nm nanotopography on the Ti substrate with microtopography that was smooth (turned) or roughened by double acid etching (DAE). The experimental implants with or without HA nanoparticles were surgically placed in rat femur and an implant push-in test was performed after two weeks of healing. The deposition of HA nanoparticles on the DAE surface increased the mechanical withstanding load by 129% and 782% as compared to the control DAE and turned implants, respectively. Micro-computed tomography-based 3D bone morphometry revealed equivalent bone volumes around the DAE implant with or without HA nanoparticles. These data suggest that the discrete deposition of HA nanoparticles accelerates the early osseointegration process, likely through increased shear bonding strengths.

(Some figures in this article are in colour only in the electronic version)

1. Introduction

The use of materials whose particulate size is decreased to below 100 nm has been increasingly anticipated to exploit

novel or significantly altered properties in the field of orthopaedic and dental biomaterials [1, 2]. Bone surface is highly mineralized with hydroxyapatite (HA) crystals and exhibits complex topography at both the microscale and the nanoscale [3]. It has been postulated that the surface topography of bone tissue may provide an optimal environment for cellular components of the skeleton and thus be used for the principle of bone implant surface designs.

³ Address for correspondence: UCLA School of Dentistry, The Weintraub Center for Reconstructive Biotechnology, Box 951668, CHS B3-087 Los Angeles, CA 90095-1668, USA.

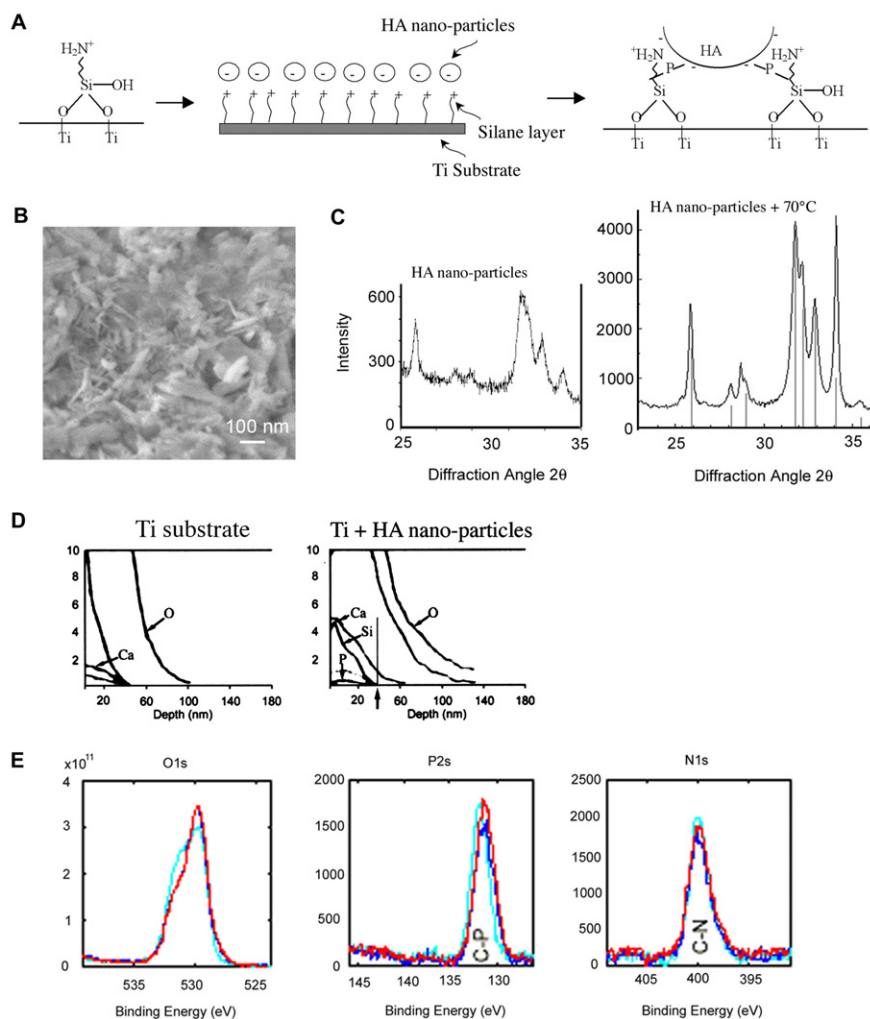


Figure 1. (A) Schematic design of the chemical bonding of HA nanoparticles to the Ti implant surface via a silane layer. (B) Field-emission SEM image of nanoparticles generated from highly crystallized HA. The longitudinal grain size of HA particles is approximately 20 nm. (C) XRD patterns of HA nanoparticles and HA colloidal material dried at 70 °C. Twenty nanometre HA nanoparticles were sintered into about a 60 nm grain-size foil. (D) Auger spectra of Ti substitute before (Ti substrate) and after the deposition of HA nanoparticles. (E) High-resolution XPS spectra of the Ti substrate deposited with HA nanoparticles. The colours/shades of grey represent data from different spots on the same sample.

When the substrate materials are soaked in acellular aqueous solutions with different ion concentrations and pH, hydroxyapatite crystals mimicking bone mineralization are precipitated [4–7]. The biomimetic hydroxyapatite has been shown to stimulate osteoblast viability and function [7–9]. Carbon nanofibres whose aspect ratio and physical dimensions are similar to crystalline HA selectively promote cellular adhesion of osteoblasts *in vitro* [10, 11]. Furthermore, nanophase ceramics and titania with 100 nm grain sizes have also been associated with increased *in vitro* adhesion of osteoblasts [12, 13] and chondrocytes [14] as well as increased function of osteoclasts [15]. These studies may suggest that the surface topography resembling bone surface HA crystals could enhance the biological activities of bone implants. However, despite these recent advances in several critical research fields, relatively few practical applications of nanotechnology have been described.

The majority of bone implant substrate materials are commercially pure titanium (Ti) or Ti alloys, whose surface

may be modified to possess microscale topography. We have envisioned a versatile nanomaterial processing protocol allowing the discrete deposition of HA nanoparticles on the Ti implant substrate with predisposing microtopography. We report here that an experimental implant with combined microscale and nanoscale surface topography by the discrete deposition of HA nanoparticles exhibited a robust biological effect and significantly increased the bone–implant bonding *in vivo* within a two-week healing time.

2. Materials and methods

2.1. Aminosilane treatment and deposition of HA nanoparticles (figure 1(A))

Commercially pure Ti substrates were prepared as either machined (turned) or by double acid-etching (DAE) treatments according to the process for fabricating Osseotite® dental implant (Implant Innovations Inc., Palm Beach Garden, FL). The Ti substrates were first cleaned in boiling water and dried

at 60–120 °C for 30 min. 3-aminopropyltriethoxysilane (APS) was dissolved in toluene (the solution concentrations tested ranged from 1% to 5.4%) at room temperature with magnetic stirring for 30 min. The cleaned Ti substrates were immersed in APS solution up to 19 h, followed by ultrasonic cleaning in toluene, toluene/methanol, methanol and distilled water. APS-treated Ti substrates were dried at room temperature for 30 min.

HA nanoparticles were purchased from Berkeley Advanced Biomaterials (Berkeley, CA) with crystalline size of 20 nm based on the supplier's data sheet. The HA nanoparticles were dispersed in ethanol to formulate 0.2 wt% colloid. The APS-treated Ti substrates were immersed in the HA nanoparticle colloid, followed by rinses in alkaline (NaOH) water and water. The HA nanoparticle-deposited Ti substrates were thermally cured at 70 °C for 30 min.

The crystallographic phase of HA nanoparticles was characterized by x-ray diffraction (XRD) (Camet Inc., Camario, CA) before and after 70 °C curing treatment. The surface chemistry of the HA nanoparticle-deposited Ti substrate was evaluated by Auger electron spectroscopy and x-ray photoelectron spectroscopy (XPS) (Anderson Materials Evaluation, Inc., MD).

2.2. Surface characterization

The Ti substrates with or without the deposition of HA nanoparticles were characterized by scanning electron microscopy (SEM). After being immersed in the HA coating solutions (0.02 wt%) for 15, 30, or 180 min, the percentage coverage of HA nanoparticles was measured. The uniformity of HA nanoparticle deposition was determined by energy dispersive spectroscopy (EDS) measured at randomly selected areas. The surface topography before and after the deposition of HA nanoparticles was measured by surface mapping microscopy (SMM) or atomic force microscopy (AFM) according to the manufacturers' instructional protocols.

2.3. Biological effect in rat femur

The biological effect of different implant topography and with or without the deposition of HA nanoparticles was tested in rat femur. Miniature cylindrical implants of commercially pure Ti (2 mm in length and 1 mm in diameter) with turned or DAE surfaces were fabricated for this study (Implant Innovations Inc., Palm Beach Garden, FL). The miniature implants were then transferred to Chemat Technology, Inc. (Northridge, CA), where the HA nanoparticle deposition process was completed as described above. The surface-modified implants were then sent back to Implant Innovations Inc., where the implants were sterilized and packed individually. The final implant specimens were sent to the Weintraub Center at UCLA and kept at room temperature until the implant surgery.

Male Sprague–Dawley rats (8–10 weeks old) were anaesthetized by 2% isoflurane gas inhalation and an implant site (1 mm in diameter and 2 mm in depth) was prepared in each femur at between 7 and 10 mm from the distal end. One cylinder implant per femur was placed by passive insertion and the wound was closed. Animals were monitored for full recovery before returning to the housing facility and allowed to heal for two weeks.

2.4. Implant push-in test

The rat femur specimens containing miniature implants were harvested two weeks after the implant placement. The femur specimens were immediately embedded in autopolymerized resin, during which the longitudinal axis of the implant was approximately aligned to be perpendicular to the horizontal plane of the resin block. The specimens were then placed on the table of an incident light microscope to measure the three-dimensional deviation angle against the direction of the implant push-in load. The electromechanical testing machine (Instron 5544) was equipped with a 2000 N load cell and a custom-made pushing rod (diameter = 0.8 mm). The implants were pushed in at a crosshead speed of 1 mm min⁻¹. The applied load and the displacement of the implant were monitored. The raw push-in value was determined by measuring the peak of the load–displacement curve. The raw push-in values were normalized against the deviation angle of the implant as follows: $Y = X/(1 + 0.017q)$ where Y is the normalized push-in value, X the raw push-in value, and q the implant deviation angle [16].

The first study evaluated the effect of APS treatment and two different conditions for HA nanoparticle coating on the implant push-in value in rats. In this study, five experimental implant groups were generated: DAE implants (the number of animals $n = 5$), DAE implants treated only with the APS (DAE/APS, $n = 3$), DAE–APS implants immersed in the HA colloidal solution for 15 min (DAE/nano-HA[15], $n = 3$), DAE/APS implants immersed in the HA colloidal solution for 180 min (DAE/nano-HA[180], $n = 5$), and DAE/APS implants with multiple HA layers (DAE/nano-HA[m], $n = 5$). In the second study, four experimental implant groups with different surface topography/chemistry were generated: turned implants ($n = 5$), turned/nano-HA implants ($n = 5$), DAE implants ($n = 5$), and DAE/nano-HA implants ($n = 5$).

The average normalized push-in value (N) of each group was calculated. The comparisons of interest were between treatment groups assessed using an unpaired Student's t -test (two-tailed). Statistical significance was reported at $p < 0.05$.

2.5. SEM and EDS analysis of the sheared implant surface

After the push-in test, the sheared implant surface was evaluated by scanning electron microscopy (SEM) and energy dispersive spectrometry (EDS). This analysis was used to validate the shear surface created by the implant push-in test. EDS analysis provides the element content of the interfacial tissue.

2.6. Micro-computed tomography (micro-CT) bone morphometry

In the following four experimental groups, turned implants ($n = 5$), turned/nano-HA implants ($n = 5$), DAE implants ($n = 5$), and DAE/nano-HA implants ($n = 5$), the three-dimensional (3D) bone volume around implants was measured by micro-CT. To fit the 15.4 mm diameter poly-ether-imid (PEI) sample holder (Scanco Medical AG, Bassersdorf, Switzerland) for the CT scan, gross cuts located 6 mm mesial and distal of the implant were performed using an exact band saw and a diamond saw band (Exakt

Table 1. Silane concentration and immersing time versus Si and N XPS concentration.

Silane concentration (wt%)	Immersion time (h)	Si (at.%)	N (at.%)
1.1	5	0.19	0.64
1.1	5	0.44	1.03
1.3	11	2.10	2.44
5.4	16	1.70	1.99
3.5	17	2.55	1.83
2.8	19	2.84	4.13

Apparatebau GmbH, Norderstedt, Germany). Cross sections were provided with an autopolymerizing resin base to align the long axis of the implant perpendicular to the x-ray beam. During the measurement the specimens were covered with phosphate-buffered saline. For each sample a total of 290 microtomographic slices with a slice increment of $8.27 \mu\text{m}$ were made from area 0.2 mm above and below the implant length. The resolution within one slice was $8 \mu\text{m} \times 8 \mu\text{m}$. For the subsequent analysis a volume of interest (VOI) of the originally measured data was selected. The bone volume within $96 \mu\text{m}$ was assessed with a custom-made evaluation program in IPL (Image Processing Language, Scanco Medical AG, Bassersdorf, Switzerland). The comparisons of interest were between treatment groups assessed using an unpaired Student's *t*-test (two-tailed). Statistical significance was reported at $p < 0.05$.

3. Results

3.1. The first layer formation: self-assembly of APS layer

The APS layer was processed by immersing the implants into a silane at room temperature for 5–19 h. After washing, the element concentrations of silicon, nitrogen, oxygen and carbon were analysed by XPS. After 11 h of immersion, the concentration of silane in the solution did not affect the final coverage/thickness of the silane layer within the range of concentrations evaluated (table 1). It was suggested that the silane layer may be saturated after 11 h of immersion.

3.2. Discrete deposition of HA nanoparticles

The nanoparticles derived from crystalline HA appeared to maintain the original crystalline structure (figure 1(B)). After the HA nanoparticle colloidal material was dried at 70°C , XRD data indicated that HA nanoparticles were sintered into approximately a 60 nm grain-sized foil (figure 1(C)). The extensive washing process and thermal drying process appeared to remove any residual toluene. The Auger analysis indicated an estimated thickness of the APS and HA nanoparticles of less than 40 nm (figure 1(D)). The self-assembled APS/HA nanoparticle bilayer was characterized by high-resolution XPS analysis, which suggested the formation of P–C bonding between the HA nanoparticles and the 'out-reached' carbon chain in the APS layer (figure 1(E)). APS reacts with the implant surface as well as HA nanoparticles and thus becomes part of the coating.

SEM evaluation at a $50\,000\times$ magnification of a DAE implant showed relatively smooth nanoscale surface areas

(figure 2(A)). After the deposition of HA nanoparticles, the presence of HA nanoparticles ranging in size from 20 to 40 nm was observed on the Ti substrate surface (figure 2(B)). There was a linear correlation between the HA coverage area (%) and the immersion time assessed in SEM (figure 2(C)). After 180 min of implant immersion in the HA nanoparticle colloid, approximately 50% of the implant surface was covered by HA nanoparticles. The EDS evaluation on the HA nanoparticle-deposited Ti substrates with different measurement areas demonstrated consistent amounts of Ca and P elements, suggesting that the HA nanoparticles were uniformly deposited (figure 2(D)).

3.3. The effect of deposition of HA nanoparticles on the microtopography of the Ti substrate

The surface topography of Ti substrates (turned or DAE) was characterized by AFM (table 2). In addition, SMM (figures 3(A) and (B)) and SEM (figures 3(C) and (D)) were further used to characterize the surface topography of DAE Ti substrate with or without the deposition of HA nanoparticles. These results indicated that the predisposing microtopography was not affected by the deposition of HA nanoparticles.

3.4. The effect of the deposition of HA nanoparticles on osseointegration

The rat femur implant push-in test was used to evaluate the rate of osseointegration (figure 4(A)). In the initial assessment, the effect of the APS treatment and the HA nanoparticle processing were examined. The normalized push-in values of control DAE implants, DAE/APS implants, DAE/nano-HA[15] implants, DAE/nano-HA[180], and DAE/nano-HA[m] implants were $18.65 \pm 5.53 \text{ N}$, $14.18 \pm 5.35 \text{ N}$, $22.63 \pm 11.09 \text{ N}$, $29.73 \pm 6.85 \text{ N}$, and $18.78 \pm 4.82 \text{ N}$, respectively (figure 4(B)). The DAE/nano-HA[180] implant group showed statistically higher implant push-in values over the control DAE implant group ($p < 0.05$) and the DAE/APS implant group ($p < 0.05$). From these data, the long-term (180 min) HA-deposition condition was selected for further evaluations.

The push-in values of two-week post-implantation of turned implants, turned/nano-HA implants, DAE implants and DAE/nano-HA implants were $3.4 \pm 2.3 \text{ N}$, $9.4 \pm 1.8 \text{ N}$, $13.1 \pm 2.0 \text{ N}$ and $30.0 \pm 8.7 \text{ N}$, respectively (figure 4(C)). A statistical significance was found between the turned and turned/nano-HA implant groups ($p < 0.05$), as well as between the DAE and DAE/nano-HA implant groups ($p < 0.001$). The surface of dissociated implants after the push-in test was evaluated by SEM (figure 4(D)). The bone tissue that remained on the implant surface appeared to be thicker on the turned/nano-HA implant than on the turned implant. The DAE/nano-HA implant appeared to be associated with a thick plate of bone tissue.

3.5. 3D bone morphometry

Five femur/implant specimens from the turned, turned/nano-HA, DAE, DAE/nano-HA implant groups were subjected to microCT scanning [17]. The 3D bone volume/tissue volume (BV/TV) within $24\text{--}48 \mu\text{m}$ vicinity around the implant was higher in the cortical bone zone than the trabecular bone zones;

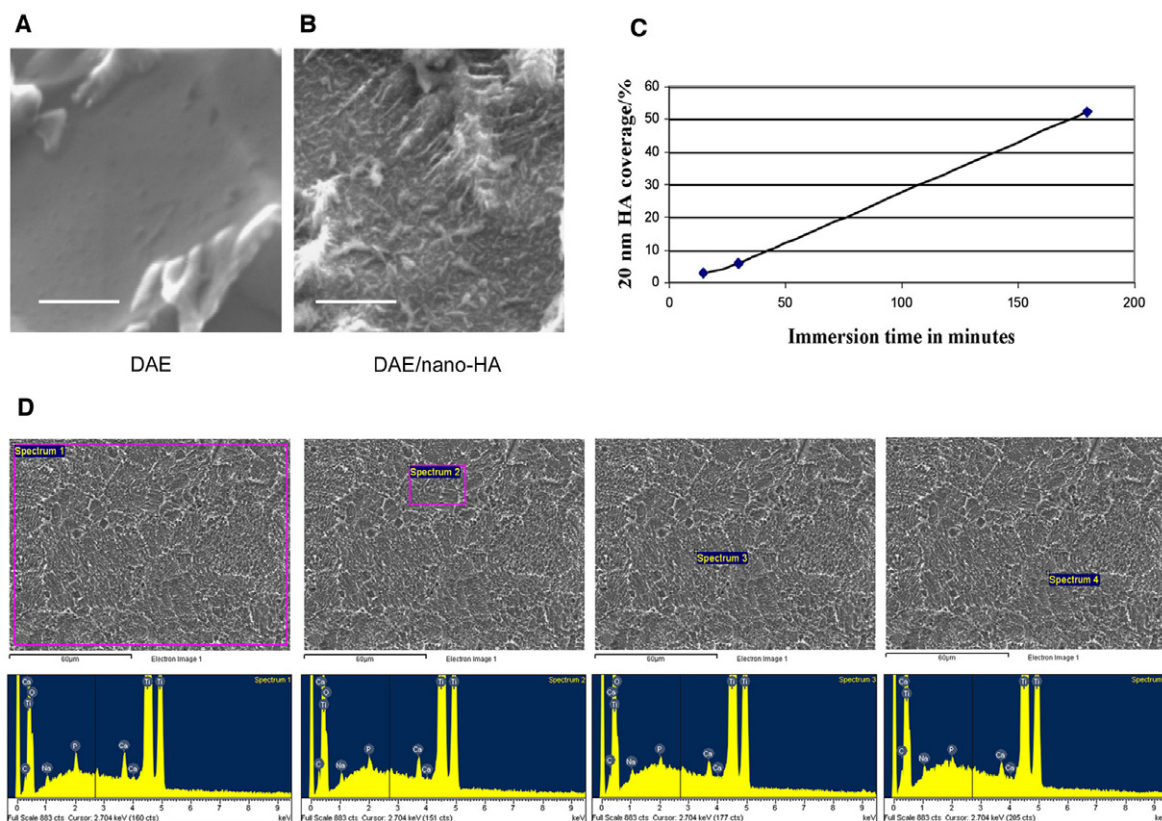


Figure 2. (A) DAE-treated Ti surface (bar = 600 nm). (B) DAE-treated Ti surface with the deposition of HA nanoparticles (bar = 600 nm). (C) HA coverage area (%) calculated from SEM versus Ti substrate immersion time in the HA nanoparticle colloidal solution. (D) EDS analyses with different spectrum sizes on DAE-treated Ti surface with the deposition of HA nanoparticles. In addition to Ti element peaks, Ca and P elements were consistently observed, suggesting that nano-HA coating was uniformly achieved.

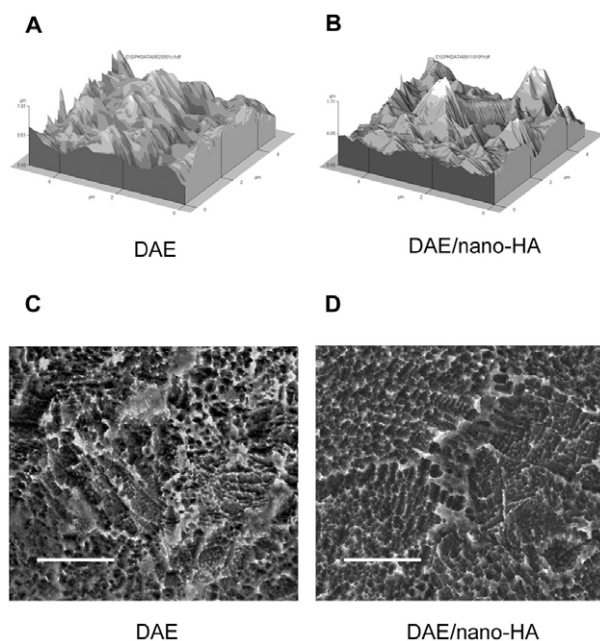


Figure 3. SMM surface topography analyses (A), (B) and SEM analyses ((C), (D): bar = 10 μm) of DAE-treated Ti substrates without ((A), (C)) or with ((B), (D)) the deposition of HA nanoparticles. No significant differences were detected.

however, the turned, turned/nano-HA, DAE, DAE/nano-HA implants did not show significant difference in the 3D BV/TV around the implant (figure 5). The turned implant group showed lower 3D trabecular bone BV/TV in the 48–72 μm and 72–96 μm zones.

4. Discussion

This report describes a novel method to modify the Ti implant surface with nanoscale HA crystal particles. SEM evaluations revealed that HA nanoparticles did not form conventional layers but rather were deposited on the Ti surface with discrete spacing. This discrete deposition of HA nanoparticles apparently contributed to the resultant nanoscale topography in the range 20–40 nm (figure 2). Castano *et al* [18] fabricated polypyrrole (PPy) thin films on tissue culture polystyrene with different pyrrole monomer concentrations, which regulated the surface nanotopography [18]. Osteoblastic bone marrow cells showed preferential adhesion to the 35–154 nm PPy but no adhesion to the 85–697 nm PPy. Osteoblastic bone marrow cells are also shown to respond to nanoscale shallow pits and grooves fabricated on the surface of polymethylmethacrylate [19]. In our study, when HA nanoparticles were deposited on the smooth (turned) Ti surface, the degree of osseointegration measured by the implant push-in test increased by 176% as compared with the

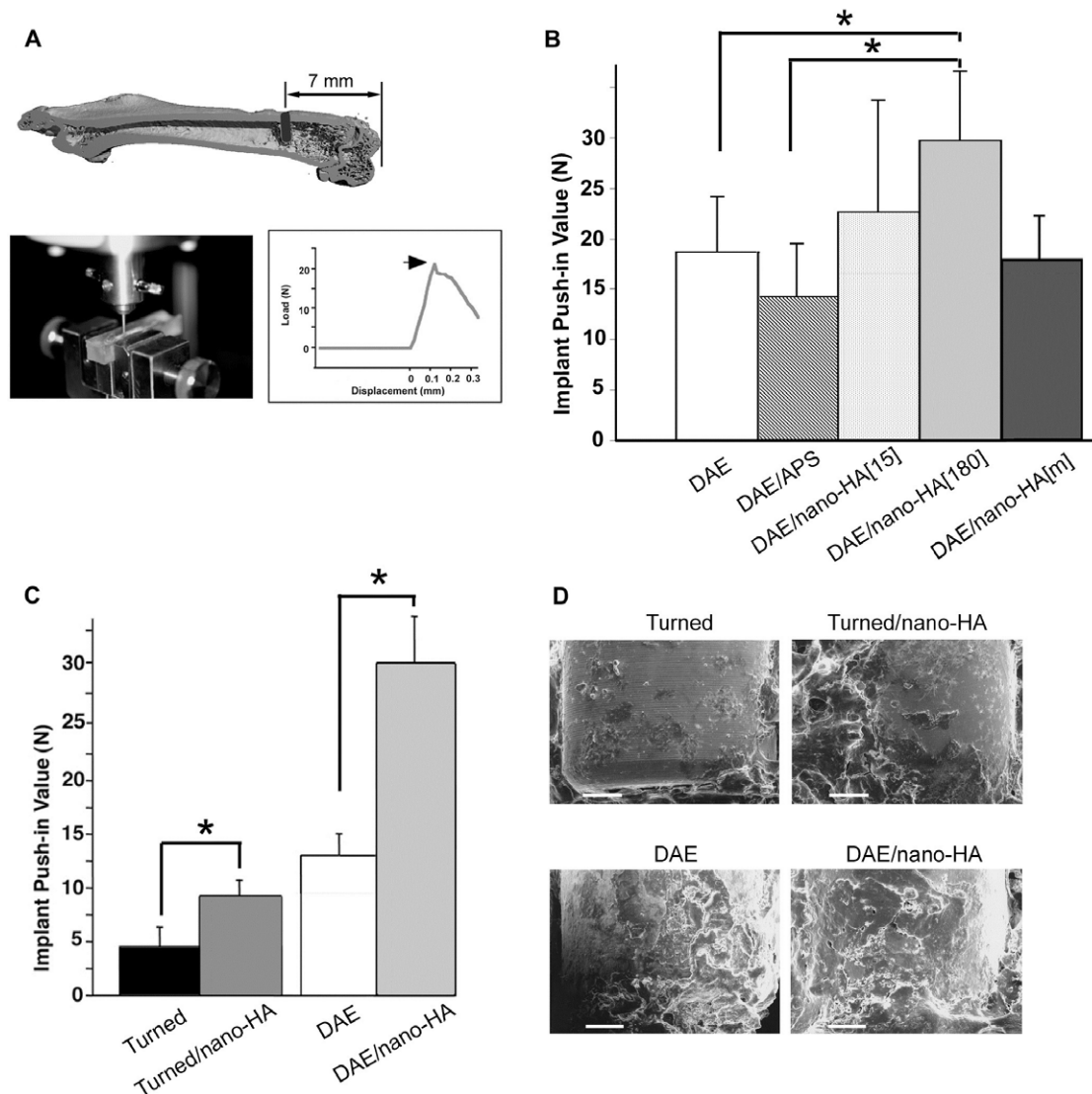


Figure 4. Rat implant push-in tests. (A) Micro-CT image of rat femur with a miniature Ti implant placed at 7 mm from the proximal end (top panel). After two weeks of healing time, the femur-implant specimen was embedded in a resin block and subjected to electromechanical loading (bottom-left panel). The maximal load prior to the implant–bone shear was used as the implant push-in value (arrow in bottom-right panel). (B) Implant push-in values measured at day 14. Test implants were DAE–Ti implants (DAE; $n = 5$), DAE–Ti implants with the first APS layer (DAE/APS; $n = 3$), APS-treated DAE–Ti implants immersed in nano-HA colloidal solution for 15 min (DAE/nano-HA[15]; $n = 3$) or 180 min (DAE/nano-HA[180]; $n = 5$), and DAE–Ti implants coated with multilayers of HA nanoparticles (DAE/nano-HA[m]; $n = 5$). Error bars indicate 1SD. * = $p < 0.05$ (C) implant push-in values of Ti implants of turned Ti implants with smooth microtopography (turned; $n = 5$), turned implants with nano-HA coating (turned/nano-HA; $n = 5$), DAE-treated Ti implants with rough microtopography (DAE; $n = 5$), and DAE implants with nano-HA coating (DAE/nano-HA; $n = 5$) measured at day 14 of implantation. Error bars indicate 1SD (one standard deviation). * = $p < 0.05$ (D) SEM analyses of the implant surface after push-in testing. Bar = 200 μm .

Table 2. AFM surface topographic analysis.

	Turned	Turned/nano-HA	DAE	DAE + APS	DAE/nano-HA		
					No. 1 ^a	No. 2 ^a	No. 3 ^a
Ra (μm)	0.04	0.04	0.14	0.17	0.16	0.15	0.16
Rrms (μm)	0.05	0.05	0.17	0.21	0.21	0.18	0.20
Rp-v (μm)	0.25	0.35	1.18	1.29	1.55	1.29	1.32

^a Independent batches were prepared for AFM analysis.

control turned implant group (figure 4(C)). The rat push-in test was developed to examine the implant–bone bonding strength in a simple model [16]. In the previous studies, the DAE

implants consistently exhibited push-in values in the range 15–20 N at day 14, whereas the turned implants showed about 50% lower push-in values at the same healing time [16, 20]. The rat

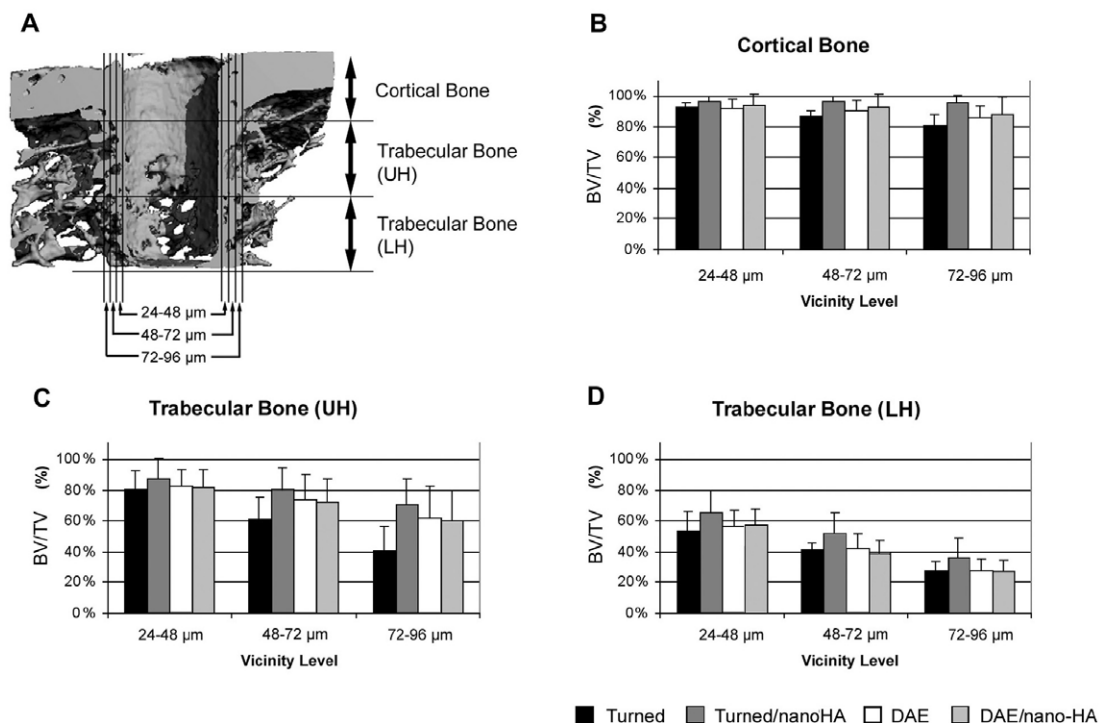


Figure 5. Three-dimensional (3D) bone morphometry using micro-CT. 3D reconstruction of bone architecture around a Ti implant integrated in rat femur (A). The implant image was digitally extracted. In each 3D data set, juxtaposing bone volume/tissue volume (BV/TV) was calculated at the cortical bone (B), upper half (UH) of the trabecular bone (C) and lower half (LH) of trabecular bone zones (D).

push-in tests conducted in this study showed comparative data, suggesting the consistency of this *in vivo* model.

The most striking biological effect was observed in the group of DAE/nano-HA implants, which combined the predisposing microtopography by treating Ti substrates with double acid etching and the discrete deposition of HA nanoparticles. As compared to the control DAE implant and turned implant groups, the DAE/nano-HA implant group showed significantly increased push-in values, by 129% and 782%, respectively. Recently, several groups have reported methods to achieve a ‘nanoscale HA coating.’ Pulsed-laser deposition was used to create an approximately 500 nm thick layer of HA droplets on commercially pure Ti or Ti-6Al-4V alloy substrate [21]. Pulsed-laser-deposited HA was found to be stable in rabbit bone for six months [22]. Another report described electrodeposition to coat a thin layer of CaP layer, which created a needle-like structure or a spherical structure of CaP of 300–500 nm [23]. It must be noted that our processing method deposited HA nanoparticles of approximately 20–40 nm, one-tenth the thickness of these recent reports. To our knowledge, this is the first report of the successful development of the deposition of HA nanoparticles on a Ti implant substrate with predisposing microtopography (table 2, figure 3), resulting in combined microtopography and nanotopography. In our system, HA nanoparticles can be multilayered by adjusting the washing protocol. We found that the multilayered HA coating decreased the predisposing microtopography by about 50% (data not shown), and did not result in any biological advantage (figure 4). Therefore, we postulate that the added discrete nanotopography through the deposition of HA nanoparticles appears to play a significant

role in this robust response and that it holds the key to the profound *in vivo* biological reaction. In addition, with these data, although the effect of HA chemistry may not be ruled out, we believe that it may have only a minor contribution to osseointegration.

SEM analysis of the implant surface after the push-in test revealed the sheared surface of implant–tissue integration (figure 4(D)). The relatively bare turned implant surface indicated that the mechanical push-in process dislodged the interface between the implant and the bone. The increasing tissue remnants on the turned/nano-HA and the DAE implant appear to suggest that the shearing occurred within the attached tissue. It must be noted that the DAE/nano-HA implant was covered by matured bone tissue, which may imply that the implant push-in test resulted in bone fracture rather than dissociation of implant from the juxtaposing bone (figure 4(D)).

The HA nanoparticles must be chemically bonded to the Ti substrate in order to prevent the release of nanoparticles that may cause cytotoxic reactions [24]. In the initial experiment, we have used a conventional tape-peel test to examine the potential delamination of HA nanoparticles. While HA nanoparticle detachment was not detected, the monitoring of nanoscale particles was not thought to be effectively achieved in this system. Alternatively we applied an indirect chemical analysis using high-resolution XPS (figure 1). The binding energy of one element is dependent on its coordination. Because the electronegativity of Si is greater than that of Ti, the O 1s peak for TiO₂ has a positive chemical shift of about +0.8 eV suggesting the generation of a Si–O–Ti bond. Testing data on the HA nanoparticle-coated Ti substrate was close

to the O 1s binding energy in Ti–O–Si moiety [25]. The P 2p binding energy was down shifted from P 2p in HA. These data support the molecular layer of the hydroxyl group (OH⁻) on the surface of Ti implanted chemically reacting with aminosilane in order to form chemical bonds by a condensation reaction (figure 1). Thus, we have interpreted that, likely due to the formation of P–C bonding between the HA nanoparticles and the ‘out-reached’ carbon chain in the APS, HA nanoparticles were covalently bonded to the Ti substrate. Covalent bonds need a larger energy to dissociate as compared to adherent bonds such as ionic or hydrogen bonds. Therefore, HA nanoparticles are not likely to be released from Ti surface under physiological circumstances.

HA has been considered a osteoconductive material and thus is used as bone grafting substitutes or carriers of bone inductive biomolecules [26, 27]. Although the formation of bone juxtaposing HA materials has been shown dependent on the porosity, pore size, pore size distribution or pore shape [28, 29], HA-coated implants are generally associated with increased bone formation. In contrast, our study of micro-CT-based 3D bone morphometry around the test implant did not differentiate the volume of bone formed juxtaposing the turned/nano-HA, DAE, and DAE/nano-HA implants (figure 5). Micro-CT analysis for 3D bone morphometry is a relatively new method [17]; however, recent studies indicate that this method may sensitively evaluate the bone–implant relationship [30, 31]. The increased push-in value of the new implant with the combination of DAE topography and the deposition of HA nanoparticles may be explained by the increased shear bonding strength between the implant surface and integrating bone tissue.

The biological mechanism responding to the combined microtopography and nanotopography generated by the discrete deposition of HA nanoparticles is unknown. The etching treatment in sulfuric acid has resulted not only in increasing the surface topography of the Ti substrate but also in generating the apparent activation energy of 67.8 kJ mol⁻¹ as derived from an Arrhenius plot [32]. The activation energy for the phase transformation of TiO₂ nanoparticles from anatase to rutile was found to be approximately 200 kJ mol⁻¹ by cobalt doping [33]. Therefore, the method we used may concurrently alter the surface energy of Ti substrates, which may then contribute to the enhanced biological response. Separately, ordered topographic features such as grooves and pits have been shown to guide cultured cell behaviours known as contact guidance [34–36]. It has been suggested that contact guidance is in part regulated by adsorption proteins such as serum components to the substrate [37]. Furthermore, the propensity of HA to adsorb serum factors [38, 39] may contribute to the robust biological response in our system. Future studies must address these factors in order to understand the biological mechanism of the discrete deposition of HA nanoparticles combined with the substrate microtopography.

5. Conclusions

The present study indicated that the newly developed nanotechnology-based material processing allowed the discrete deposition of HA nanoparticles that were chemically bonded to the Ti substrate. The deposition of HA nanoparticles did not alter the predisposing microtopography of the Ti

substrate; however, it created novel nanoscale topography. Finally, this new versatile possessing protocol demonstrated significantly accelerated bone–implant integration.

Acknowledgments

We thank Dr Jiankai Liu of Chemat Technology, Inc., for valuable suggestions during the initial prototype development, and Dr John E Davies of the University of Toronto, for constructive criticisms on the surface characterization. We also thank Drs James Kenealy, Bruce Berckmans and Prabhu Gubbi of Biomet 3i for their technical assistance in SEM and SMM. This study was supported by the NIH SBIR program (1R43 DE14927). This investigation was conducted in part in a facility constructed with support from Research Facilities Improvement Program Grant Number C06 RR014529 from the National Center for Research Resources, National Institutes of Health.

References

- [1] Stevens M M and George J H 2005 Exploring and engineering the cell surface interface *Science* **310** 1135–8
- [2] Tasker L H, Sparey-Taylor G J and Nokes L D 2007 Applications of nanotechnology in orthopaedics *Clin. Orthop. Relat. Res.* **456** 243–9
- [3] Palin E, Liu H and Webster T J 2005 Mimicking the nanofeatures of bone increases bone-forming cell adhesion and proliferation *Nanotechnology* **16** 1828–35
- [4] Kokubo T, Kushitani H, Sakka S, Kitsugi T and Yamamuro T 1990 Solutions able to reproduce *in vivo* surface-structure changes in bioactive glass-ceramic A-W *J. Biomed. Mater. Res.* **24** 721–34
- [5] Filgueiras M R, La Torre G and Hench L L 1993 Solution effects on the surface reactions of a bioactive glass *J. Biomed. Mater. Res.* **27** 445–53
- [6] Chou Y F, Chiou W A, Xu Y, Dunn J C and Wu B M 2004 The effect of pH on the structural evolution of accelerated biomimetic apatite *Biomaterials* **25** 5323–31
- [7] Oh S H, Finones R R, Daraio C, Chen L H and Jin S 2005 Growth of nano-scale hydroxyapatite using chemically treated titanium oxide nanotubes *Biomaterials* **26** 4938–43
- [8] Matsuoka H, Akiyama H, Okada Y, Ito H, Shigeno C, Konishi J, Kokubo T and Nakamura T 1999 *In vitro* analysis of the stimulation of bone formation by highly bioactive apatite- and wollastonite-containing glass-ceramic: released calcium ions promote osteogenic differentiation in osteoblastic ROS17/2.8 cells *J. Biomed. Mater. Res.* **47** 176–88
- [9] Chou Y F, Huang W, Dunn J C, Miller T A and Wu B M 2005 The effect of biomimetic apatite structure on osteoblast viability, proliferation, and gene expression *Biomaterials* **26** 285–95
- [10] Price R L, Waid M C, Haberstroh K M and Webster T J 2003 Selective bone cell adhesion on formulations containing carbon nanofibres *Biomaterials* **24** 1877–87
- [11] Price R L, Ellison K, Haberstroh K M and Webster T J 2004 Nanometer surface roughness increases select osteoblast adhesion on carbon nanofibre compacts. *J. Biomed. Mater. Res. A* **70** 129–38
- [12] Webster T J, Ergun C, Doremus R H, Siegel R W and Bizios R 2000 Specific proteins mediate enhanced osteoblast adhesion on nanophase ceramics *J. Biomed. Mater. Res.* **51** 475–83
- [13] Webster T J, Siegel R W and Bizios R 1999 Osteoblast adhesion on nanophase ceramics *Biomaterials* **20** 1221–7

- [14] Kay S, Thapa A, Haberstroh K M and Webster T J 2002 Nanostructured polymer/nanophase ceramic composites enhance osteoblast and chondrocyte adhesion *Tissue Eng.* **8** 753–61
- [15] Webster T J, Ergun C, Doremus R H, Siegel R W and Bizios R 2001 Enhanced osteoclast-like cell functions on nanophase ceramics *Biomaterials* **22** 1327–33
- [16] Ogawa T, Ozawa S, Shih J H, Ryu K H, Sukotjo C, Yang J M and Nishimura I 2000 Biomechanical evaluation of osseous implants having different surface topographies in rats *J. Dent. Res.* **79** 1857–63
- [17] Butz F, Ogawa T, Chang T L and Nishimura I 2006 Three-dimensional bone-implant integration profiling using micro-computed tomography *Int. J. Oral Maxillofac. Implant.* **21** 687–95
- [18] Castano H, O'Rear E A, McFetridge P S and Sikavitsas V I 2004 Polypyrrole thin films formed by admicellar polymerization support the osteogenic differentiation of mesenchymal stem cells *Macromol. Biosci.* **4** 785–94
- [19] Dalby M J, McCloy D, Robertson M, Wilkinson C D and Oreffo R O 2006 Osteoprogenitor response to defined topographies with nanoscale depths *Biomaterials* **27** 1306–15
- [20] Ozawa S, Ogawa T, Iida K, Sukotjo C, Hasegawa H, Nishimura R D and Nishimura I 2002 Ovariectomy hinders the early stage of bone-implant integration: histomorphometric, biomechanical, and molecular analyses *Bone* **30** 137–43
- [21] Blind O, Klein L H, Dailey B and Jordan L 2005 Characterization of hydroxyapatite films obtained by pulsed-laser deposition on Ti and Ti-6AL-4v substrates *Dent. Mater.* **21** 1017–24
- [22] Peraire C, Arias J L, Bernal D, Pou J, Leon B, Arano A and Roth W 2006 Biological stability and osteoconductivity in rabbit tibia of pulsed laser deposited hydroxylapatite coatings *J. Biomed. Mater. Res.* **77** 370–9
- [23] Richard D, Dumelie N, Benhayoune H, Bouthors S, Guillaume C, Lalun N, Balossier G and Laurent-Maquin D 2006 Behavior of human osteoblast-like cells in contact with electrodeposited calcium phosphate coatings *J. Biomed. Mater. Res.* **79** 108–15
- [24] Nel A, Xia T, Madler L and Li N 2006 Toxic potential of materials at the nanolevel *Science* **311** 622–7
- [25] Lin Y L, Wang T J and Yong J 2002 Surface characteristics of hydrous silica-coated TiO₂ particles *Powder Technol.* **123** 194–8
- [26] Gosain A K 2005 Biomaterials for reconstruction of the cranial vault *Plast. Reconstr. Surg.* **116** 663–6
- [27] Kwon B and Jenis L G 2005 Carrier materials for spinal fusion *Spine J.* **5** 224S–30
- [28] Chang B S, Lee C K, Hong K S, Youn H J, Ryu H S, Chung S S and Park K W 2000 Osteoconduction at porous hydroxyapatite with various pore configurations *Biomaterials* **21** 1291–8
- [29] Hing K A, Best S M, Tanner K E, Bonfield W and Revell P A 1999 Quantification of bone ingrowth within bone-derived porous hydroxyapatite implants of varying density *J. Mater. Sci. Mater. Med.* **10** 663–70
- [30] Simank H G, Stuber M, Frahm R, Helbig L, van Lenthe H and Muller R 2006 The influence of surface coatings of dicalcium phosphate (DCPD) and growth and differentiation factor-5 (GDF-5) on the stability of titanium implants *in vivo* *Biomaterials* **27** 3988–94
- [31] Otsuki B, Takemoto M, Fujibayashi S, Neo M, Kokubo T and Nakamura T 2006 Pore throat size and connectivity determine bone and tissue ingrowth into porous implants: three-dimensional micro-CT based structural analyses of porous bioactive titanium implants *Biomaterials* **27** 5892–900
- [32] Ban S, Iwaya Y, Kono H and Sato H 2005 Surface modification of titanium by etching in concentrated sulfuric acid *Dent. Mater.* **22** 1115–20
- [33] Barakat M A, Hayes G and Shah S I 2005 Effect of cobalt doping on the phase transformation of TiO₂ nanoparticles *J. Nanosci. Nanotechnol.* **5** 759–65
- [34] Brunette D M 1988 The effects of implant surface topography on the behaviour of cells *Int. J. Oral Maxillofac. Implant.* **3** 231–46
- [35] Curtis A and Wilkinson C 1997 Topographical control of cells *Biomaterials* **18** 1573–83
- [36] Matsuzaka K, Walboomers F, de Ruijter A and Jansen J A 2000 Effect of microgrooved poly-L-lactic (PLA) surfaces on proliferation, cytoskeletal organization, and mineralized matrix formation of rat bone marrow cells *Clin. Oral Implant. Res.* **11** 325–33
- [37] Teixeira A I, Abrams G A, Bertics P J, Murphy C J and Nealey P F 2003 Epithelial contact guidance on well-defined micro- and nanostructured substrates *J. Cell. Sci.* **116** 1881–92
- [38] Sawyer A A, Hennessy K M and Bellis S L 2007 The effect of adsorbed serum proteins, RGD and proteoglycan-binding peptides on the adhesion of mesenchymal stem cells to hydroxyapatite *Biomaterials* **28** 383–92
- [39] Woo K M, Seo J, Zhang R and Ma P X 2007 Suppression of apoptosis by enhanced protein adsorption on polymer/hydroxyapatite composite scaffolds *Biomaterials* **28** 2622–30